A computational optimization study of a self-expandable transcatheter aortic valve

Sara Barati[1], Nasser Fatouraee[1*], Malikeh Nabaei[1], Francesca Berti[2], Lorenza Petrini[3], Francesco Migliavacca[2], Jose Felix Rodriguez Matas[2*]

1. Biological Fluid Dynamics Research Laboratory, Biomedical Engineering Department, Amirkabir University of Technology, 350 Hafez Ave, Tehran, Iran

2. Laboratory of Biological Structure Mechanics (LaBS), Department of Chemistry, Materials, and Chemical Engineering "Giulio Natta", Politecnico di Milano, Piazza Leonardo da Vinci 32, 20133 Milan, Italy

3. Department of Civil and Environmental Engineering, Politecnico di Milano, Piazza Leonardo da Vinci 32, 20133 Milan, Italy

Abstract

Developing an efficient stent frame for transcatheter aortic valves (TAV) needs thorough investigation in different design and functional aspects. In recent years, most TAV studies have focused on their clinical performance, leaflet design, and durability. Although several optimization studies on peripheral stents exist, the TAV stents have different functional requirements and need to be explicitly studied. The aim of this study is to develop a cost-effective optimization framework to find the optimal TAV stent design made of Ni-Ti alloy. The proposed framework focuses on minimizing the maximum strain occurring in the stent during crimping, making use of a simplified model of the stent to reduce computational cost. The effect of the strut cross-section of the stent, i.e., width and thickness, and the number and geometry of the repeating units of the stent (both influencing the cell size) on the maximum strain is investigated. Three-dimensional simulations of the crimping process are used to verify the validity of the simplified representation of the stent, and the radial force has been calculated for further evaluation. The results suggest the key role of the number of cells (repeating units) and strut width on the maximum strain and, consequently, on

* Corresponding authors: Nasser Fatouraee and Jose Felix Rodriguez Matas
E-mail address: nasser@aut.ac.ir; josefelix.rodriguezmatas@polimi.it

the stent design. The difference in terms of the maximum strain between the simplified and the 3D model was less than 5%, confirming the validity of the adopted modeling strategy and the robustness of the framework to improve the TAV stent designs through a simple, cost-effective, and reliable procedure.

Keywords: Transcatheter aortic valve, Finite element analysis, Optimization, Genetic algorithm, Shape memory alloy, Ni-Ti alloys

1 Introduction

Since the first successful transcatheter aortic valve (TAV) implantation (TAVI) in 2002 [1], the minimally invasive procedure to implant a heart valve has been recognized as one of the main options for the treatment of high-risk patients with severe aortic stenosis [2,3]. The need to design a durable, practical, and cost-efficient device has created a rapidly growing research field. In recent years, a large number of new designs have been introduced and analyzed to improve the life expectancy and quality for the patients receiving these types of valves [4–8]. Due to the minimally invasive nature of this new procedure, valve designs can be improved to become the main procedure for treating critical valve disease and be available even for younger, lower-risk patients who might not be able to undergo open-heart surgery [9–11].

One of the most critical aspects of designing the TAV is the structure of the stent. The stent should be able to provide the structural support for the aortic valve as long as possible and withstand a high range of strain during the crimping and implantation steps. Two types of stents are mainly used for TAVI; self-expandable and balloon-expandable stents. Self-expandable stents are made of Nickel-Titanium (Ni-Ti) alloy, a shape memory alloy that, according to the working temperature, can endure elastic strains over 10% (for biomedical devices, it is designed to exploit

superelasticity at body temperature). Furthermore, the large elastic strain provided by Ni-Ti can reduce the risk of stent damages during crimping and deployment [12]. On the contrary, balloon-expandable stents, made of ductile materials such as Cobalt-Chromium alloys, need to be plastically deformed (endurance up to 0.3%) during the deployment phase [13].

In complex biologic systems like heart valves, it can be expensive, or very difficult, to measure some of the TAV performance data in vivo [14], such as the contact pressure the device exerts on the surrounding tissue that could lead to post-intervention complications as Left Bundle Branch Block (LBBB) [15]. The geometric complexity and manufacturing costs limit the use of standardized tests required for the in-vitro evaluation of stents. In this regard, the finite element method is a well-established numerical methodology for dealing with the complex problem of estimating the function, durability, and failure modes of devices [16]. Many studies have employed this method for function analysis [17–20] and design optimization analysis [21–27] of coronary and peripheral arterial stents. The data acquired from these studies have been useful in improving the design of stents over the years. Since the recent introduction of TAV, several clinical trials and researches concerning the functionality of these devices have been started [28–34]. Besides, several studies on the performance of the TAV devices in idealized anatomical [35,36] or patient-specific [37–39] aortic root have been performed. However, some aspects are not thoroughly investigated yet. To the best of our knowledge, only a few studies address the design and material optimization of TAV stents [40–42]. Rocatello et al. [40] have proposed a framework for optimizing two design factors of the TAV stent regarding the conduction abnormalities and paravalvular regurgitation. Their results suggest that a large proximal diameter and high first cell improve the device's anchorage and reduce contact pressure. Bosi et al. [41] optimized the material properties and thickness of the aortic root by performing patient-specific simulations of cobalt-

chromium TAV stent. The numerical method was validated by comparing the paravalvular leakage estimated in simulation with the post-TAVR images. Carbonaro et al. [42] proposed a multi-objective optimization framework for the shape and cross-section of the TAV stents. The pullout force, maximum stress exerted on the aortic wall, and the maximum contact pressure in the left ventricle outflow region of the aortic root was evaluated for healthy and diseased scenarios.

In this study, a novel computationally cost-effective optimization framework to optimize the design of a self-expandable TAV stent is presented. Using this approach, the effects of strut width and thickness and the number and characteristics of the repeating cell patterns of the stent on the maximum strain developed during the crimping phase of implantation are investigated. The range of variation of these design parameters has been chosen based on typical commercially available self-expandable stents. Different mechanical properties associated with two Ni-Ti alloys were employed to evaluate their role in affecting the maximum strain value. The optimization was then verified utilizing 3D numerical simulations performed on the optimized designs to ensure that the results were reliable.

2 Materials and Methods

2.1 Stent Geometry

The stent is constructed of several repetitive patterns in the circumferential direction connected with links. Each pattern consists of a number of cells of variable length in the longitudinal direction, made of four struts. Fig. 1a shows the different structural elements for a typical self-expandable stent. The stent geometry was generated from the symmetric half of the pattern, referred to as “string” (see Fig. 1b) that was repeated in the circumferential direction following an imposed diameter profile, $D(x)$, of a typical commercially available stent shown in Fig. 1c. The

geometry of the string was parametrized by the height of the stent (H), and the number of cells in the longitudinal direction (n) in addition to the number of pattern repetitions in the circumferential direction (p) required to generate the stent in 3D. The frame height (H) is fixed at 50 mm, corresponding to an average value of the height of the commercially available stents of size 26 mm. The length of the cells within a single pattern was parametrized with three different lengths, as shown in Fig. 1b. The most proximal cell length (L_1), the length of intermediate cells (L_2), and the length of the most distal cell (L_3) which is obtained as

$$L_3 = \mathrm{H} - L_1 - (n-2)L_2. \tag{1}$$

The choice of considering the same length for intermediate cells, L_2, has followed the results of a preliminary analysis using the surrogate model (the 1D string model). The analysis considered the length of each cell as an independent optimization variable. Results from the analysis indicated that the optimal solution consisted of stents with the middle cells of similar lengths in most cases. Further, changes in these lengths didn't imply significant changes in the maximum strain (results not shown). However, the presented methodology can be applied to more complex parametrizations of the stent without further complications. The shape of the different cells was described using a cubic spline with zero slopes at the endpoints and the coordinates of the mid-point ($y(x_i)$) (see Fig. 1b) was defined according to the diameter profile shown in Fig. 1c (see Supplementary Material-1 for the definition of the diameter profile used in this study) as follows:

$$y(x_i) = \frac{\pi D(x_i) - 2pw}{2p} \tag{2}$$

where x_i corresponds to the position of the mid-point of the cell and w is the strut width. The optimization of the cell geometry was performed, leaving H, and the diameter profile in Fig. 1c fixed while allowing changes in n, p, L_1 and L_2, as well as the strut width (w) and thickness (t).

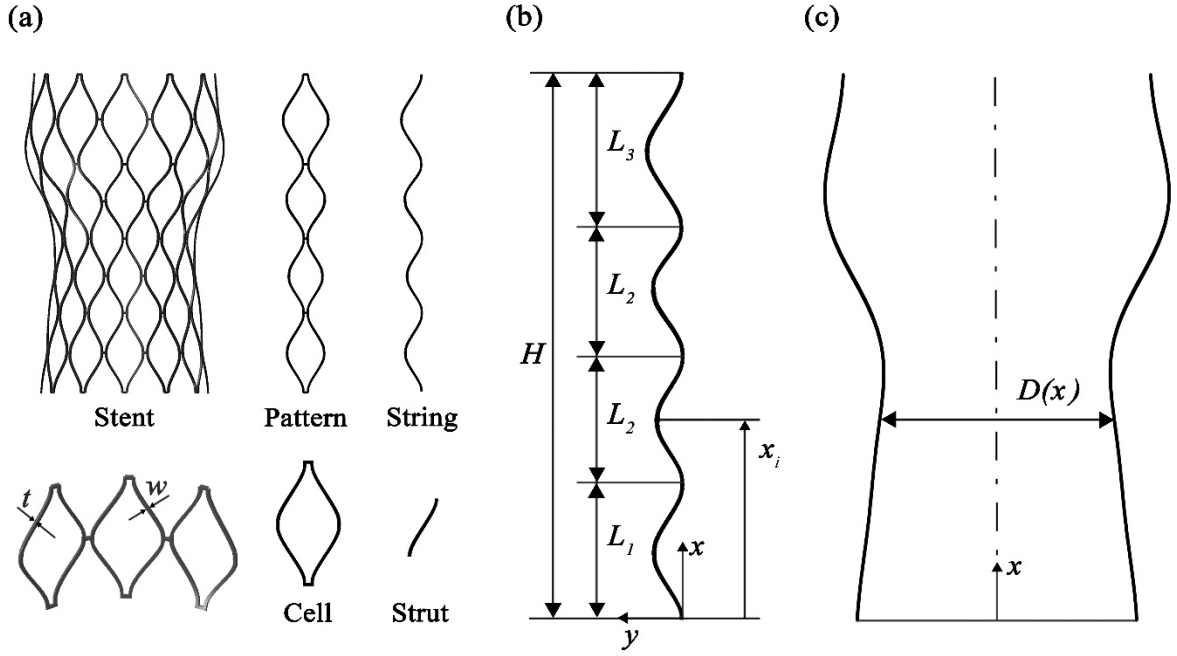

Fig. 1. Stent components; repeating patterns in the circumferential direction, strings, cells, and struts

2.2 Mechanical Test Experiments

Stent material was modeled as a shape memory alloy following the formulation proposed by Auricchio and Taylor [43]. The mechanical properties of Ni-Ti alloys depend on the manufacturing process [44]. To investigate the effect of material properties on stent design optimization, two sets of material parameters were used. The first set (M1) was derived from the tensile tests performed on two laser-cut samples of available medical Ni-Ti alloys, while the second (M2) was adopted from the literature to obtain a similar global behavior [45], but with a symmetric material (tension-compression). Two types of tensile test samples were used for material M1, as shown in Fig. 2b.

Standard dog-bone shape samples were used for material characterization, whereas string-like samples, used in the optimization procedure, were utilized for model verification.

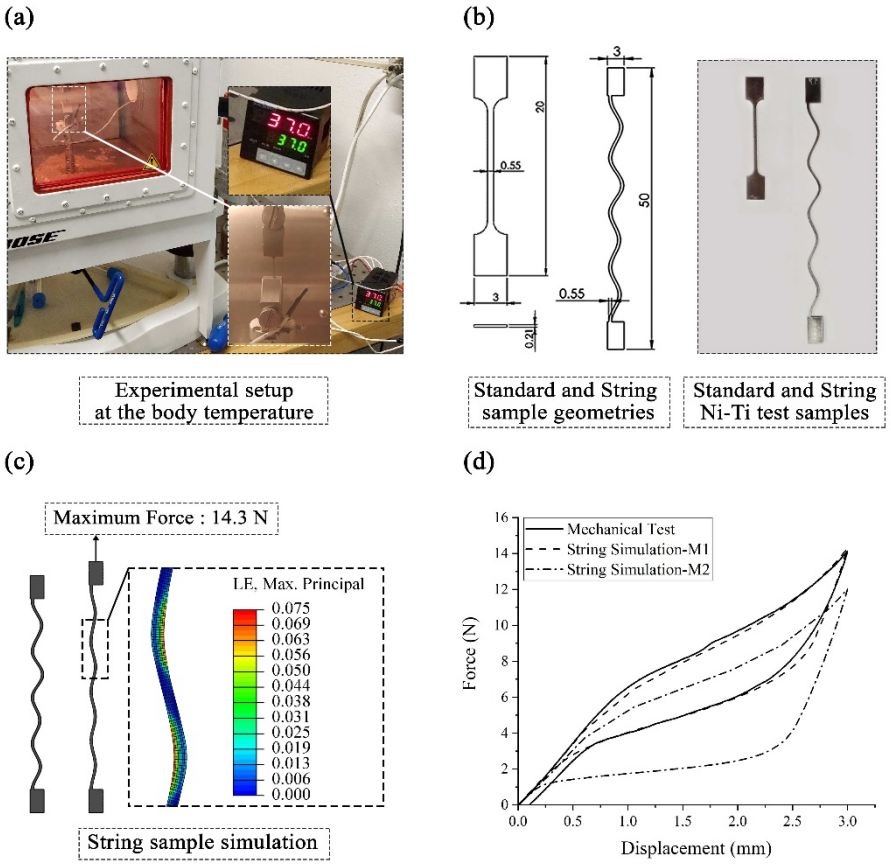

Fig. 2. a) The experimental setup for tensile test on Ni-Ti samples. The tests were conducted in a temperature-controlled chamber. b) String-like and standard dog-bone geometries and laser cut samples used for mechanical tensile tests (not in scale). Both samples are 0.21 mm thick and have a constant width of 0.55 mm along the testing length. c) The string sample simulation was performed with the boundary conditions, similar to the tensile test. The inset shows the strain contour on the string. d) Experimental and simulated force–displacement curve for the string sample; material properties M1and M2 are reported in Table 1.

The tensile tests were conducted using a Bose EnduraTEC ELF 3200 Uniaxial Testing System, equipped with a temperature-controlled chamber set at 37±1 °C (Fig. 2a). The testing procedure consisted of tension loading up to 3 mm and then unloading down to the initial configuration at a displacement rate of 0.3 mm/s corresponding to a maximum strain rate in the stent structures of

less than 0.045 s^{-1} [44]. The material properties extracted from the force–displacement curves of the standard dog-bone sample are reported in Table 1 (column M1).

The asymmetric behavior of the Ni-Ti alloy was estimated, assuming a value for the start of transformation loading in compression of 525 MPa, according to data reported in the literature [18].

Table 1 Ni-Ti alloys material properties

Parameter	Material M1	Material M2
Austenite Elasticity (MPa)	50000	45000
Austenite Poisson's Ratio	0.3	0.3
Martensite Elasticity (MPa)	20000	22500
Martensite Poisson's Ratio	0.3	0.3
Transformation Strain	0.0364	0.0426
Start of Transformation Loading (MPa)	350	310
End of Transformation Loading (MPa)	400	335
Reference Temperature (°C)	37	37
Start of Transformation Unloading (MPa)	250	100
End of Transformation Unloading (MPa)	150	75

The resultant material properties were then used to perform a finite element simulation involving the string sample geometry. The constitutive model available in ABAQUS/Standard 2019 (Dassault Systèmes Simulia Corp., Providence, RI, USA) for superelastic materials was used. The string was fixed at one end, and the displacement boundary condition was applied on the other end, using a Multi-Point Constraint (MPC) to mimic the actual machine grips. The force–displacement curves from the simulation and the mechanical test of the string sample were compared to verify the goodness of the material model parameters. Fig. 2d shows the excellent agreement between the simulation and the experiments for the string-like sample (R^2=0.99). The figure also shows the results for the string-like sample for material M2. The influence of the material parameters is evident, with M2 material showing significantly more hysteresis and lower stresses for the same strain value than material M1.

2.3 Optimization Methodology

The optimization problem aimed at finding the optimal stent parameters: n, p, L_1, L_2, t, and w that minimize the maximum strain ($\varepsilon_{\max}$) in the stent during crimping. The fatigue life of the Ni-Ti alloys depends mainly on the strain [46,47], and our focus in this study was on providing an optimization framework for the structural performance of the stent, regardless of the aortic root geometry. To reduce the computational costs, the optimization was based on the string geometry shown in Fig. 1b (see below for details on this surrogate model). The constrained optimization problem was defined as follows:

$$\begin{gathered} \min_{n,p,L_1,L_2,t,w} \varepsilon_{\max} \\ s.t. \\ L_2 - L_1 \leq 0 \\ 2L_1 + (n-2)L_2 - H \leq 0 \\ \frac{H}{10} \leq L_1 \leq \frac{H}{2};\ L_2 \geq \frac{H}{10} \end{gathered} \tag{3}$$

The bound limits in L_1 and L_2 were chosen based on the geometry of similar commercially available stents. The remaining constraints limit the searching space in L_1 and L_2. Further, to avoid the stent material to exceed the material yielding strain, which was assumed to be equal to 0.1 [48], the maximum acceptable strain was set to be strictly less than 0.1.

To reduce the complexity of the optimization problem, it was decided to limit the searching variables (continuous varying variables) to parameters L_1 and L_2 only, while the remaining parameters were varied according to a full factorial design of experiments (DoE) with different levels for n, p, t, and w as shown in Table 2.

Table 2 Geometric parameters and their corresponding values considered in the DoE

Parameter	Value
Number of cells, *n*	3, 4, 5
Number of pattern repetitions, *p*	10,12,14,16

Strut thickness, t (mm)	0.3, 0.5
Strut width, w (mm)	0.35, 0.5

The ranges of values in Table 2 were chosen based on commercially available transcatheter valves of size 26 mm. Parameter combinations in Table 2 defined 48 different stent configurations for which the cell lengths L_1 and L_2 were optimized according to the problem (3). From these 48 optimal design candidates, those having the minimum $\varepsilon_{\max}$ were selected. This procedure was performed for materials M1 and M2 for a total of 96 case scenarios to be optimized, shown in Fig. 3.

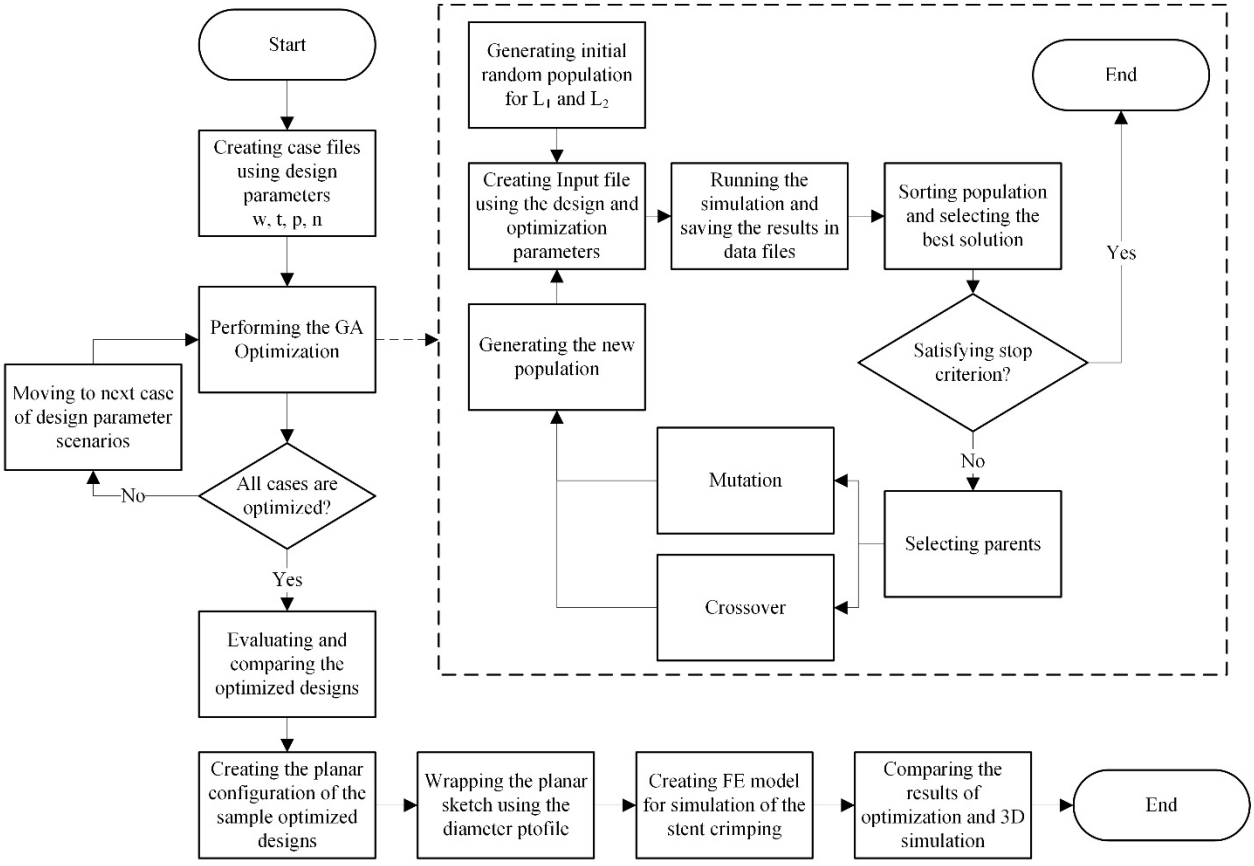

Fig. 3. Flow chart of the optimization methodology implemented in this study. The box in dashed lines represents the optimization of each case scenario of the DoE.

A Matlab script (MathWorks, Inc., MA, USA) was used to create the string geometry according to the parametrization shown in Fig. 1b and to generate the finite element model of the string as described in the following. The geometry was discretized with linear Timoshenko beam elements (average element size 0.08 mm) with a rectangular cross-section ($w \times t$). The element size was chosen such that the maximum strain varied less than 1% between two consecutive meshes where the element size has been halved. The boundary conditions were defined to reproduce the symmetry of the pattern in the circumferential direction (see Fig 1a). In brief, the origin of the string (the node in the left end) was pinned, whereas the nodes coincident with the valleys of the string, corresponding to the end of each cell, were constrained to move in the *y*-direction while being free to move in the *x*-direction (see Fig. 4).

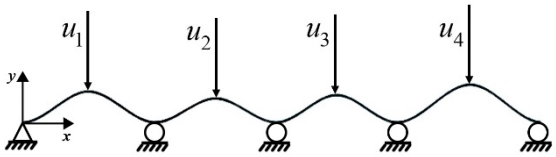

Fig. 4. The optimization simulation boundary conditions. The corresponding displacement boundary condition was applied to each joint to mimic the stent crimping.

To simulate the crimping process, the radial displacement of the stent during crimping was translated into a circumferential displacement u_i imposed at the mid-node of each cell, as shown in Fig. 4. The value of the displacement depends on the diameter profile $D(x)$, the crimping diameter D_c and the number of patterns p as follows

$$u_i = \pi \frac{D(x_i) - D_c}{2p} \quad . \tag{4}$$

A D_c of 6 mm was used. This diameter is consistent with an 18Fr catheter size used for the commercially available stents of size 26 mm. All finite element string computations were carried out using the ABAQUS/Standard 2019 implicit solver. A finite element model of a typical string used in the analyses can be found in the supplementary materials (Supplementary Material-2). The Matlab script to generate the finite element model according to the parametrization described in Fig. 1 is also available in Supplementary Material-3.

The optimization problem, Eq. (3), was solved using the Genetic Algorithm (GA), a robust and reliable approach for nonlinear problems that, with an appropriate setup, can provide a global optimal point [49]. The GA was run with 150 generations and a population size of 10 members. A uniform crossover was applied to 40%, and a one-bit mutation was applied to 10% of the population. The parent selection was based on elite selection, and the stop criterion was the maximum number of generations. This combination was found to ensure the optimization problem's convergence to a valid answer while minimizing the number of finite element simulations. Besides, the increase in the number of generations or the population didn't change the optimization results. This combination resulted in 760 finite element simulations of string crimping per optimization. Gradient-based optimization algorithms, i.e., sequential quadratic programming (sqp), can also be used for this optimization problem. However, although these algorithms are globally convergent, they do not guarantee convergence to a global optimum. Identifying a potential global optimum with gradient-based optimizers requires multiple runs with different starting points, significantly increasing the total computing time.

2.4 Three-dimensional Simulations

Three-dimensional models of the optimized stents were created to compare the maximum strain obtained from the simplified model with the full 3D model of the same stent design and verify the

accuracy of the simplified 1D model. Besides, the effect of different design parameters on the radial force obtained as a by-product of the 3D simulation was also studied for completeness. To generate the 3D model, first, a planar sketch of the optimized stent was created with the computer-aided design software SolidWorks (Dassault Systèmes SolidWorks Corp., Waltham, MA). Then, a Matlab code was used to wrap the planar sketch using the stent diameter profile defined in Fig. 1c. The resultant 3D stent was then crimped using 12 parallel rigid planes up to the crimping radius equivalent to the 18Fr catheter size. Fig. 5 shows the 3D representation of an optimized stent together with the planes used for the crimping.

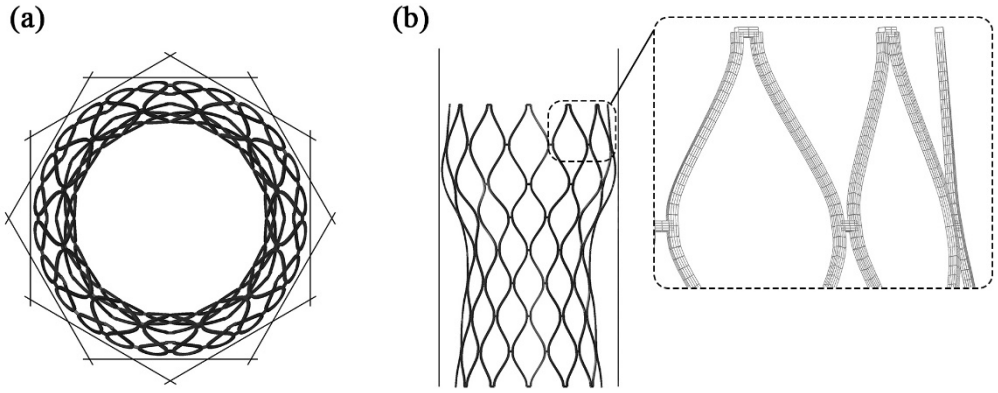

Fig. 5. The 3D simulated model of the case with parameters: w=0.35 mm, t=0.3 mm, n=4, and p=12. a) Top view; Twelve planes were used to crimp the stent. b) Front view; The inset shows a rendering of the 3D beam mesh, demonstrating the discretization of the element by 25 integration points.

The stent was meshed using quadratic beam elements with 25 (5x5) Gauss points in the cross-section (see the inset in Fig. 5b). A mesh sensitivity analysis was performed to ensure the balance of cost and accuracy of simulations in terms of the maximum strain attained during crimping, resulting in an average element size of 0.5 mm (Supplementary Material-4). The finite element simulation was performed using the Abaqus explicit solver. Crimping is performed in 1s with mass scaling to target a minimum time increment of 10^{-6} s, together with mass proportional Rayleigh

damping with $\alpha = 100$ 1/s to minimize dynamic effects. For this combination of parameters, the kinetic energy amounted to less than 1% of the internal energy respecting the quasi-static deformation assumption. Frictionless hard-contact was defined between the stent and the rigid crimping planes, and self-contact between the stent struts.

3 Results

The results of this study are presented in two main parts. First, results from the optimization procedure performed with the simplified planar string model of the stent. Secondly, the results of the full 3D simulations performed on the optimized stent configuration. The primary purpose of the 3D simulation was to assess the feasibility of using the simplified representation of the stent to drive the device optimization. Besides, the 3D simulations were used to compute the radial force of the stent. The optimization of each case scenario lasted from 3 to 26 hours, depending on the number of cells and pattern repetitions of the string, on a computing node with two Intel Xeon quad-cores at 2.4 GHz and 24 GB RAM.

3.1 Optimization

The optimum value of L_1 and L_2, together with the achieved minimum-maximum strain for all case scenarios, are summarized in Supplementary Material-5. Table 3 shows the optimal stent configurations for materials M1 and M2.

For both materials, the optimized stent had three cells and 16 pattern repetitions, with a cross-section of 0.35mm width and 0.3 mm thick (see Table 3). The main difference is found in the maximum strain during crimping, which was 0.059 (1.69 safety factor against yielding limit) for material M1 and 0.056 (1.78 safety factor against yielding limit) for material M2, implying an improvement of 5% with respect to material M1. The results also showed that the minimum was

identified after 80 iterations (generation), with the optimization process being able to reduce the maximum strain between 2% and 53%.

Table 3 Optimized designs for tested and adopted materials.

Material	Model Name	Design Parameters				Optimized Parameter		Resultant Design Parameter	Object Function
		Width (mm)	Thickness (mm)	Cells	Patterns	L_1 (mm)	L_2 (mm)	L_3 (mm)	Maximum Strain
M1	C1-M1-12	0.35	0.3	3	16	16.70	14.20	19.10	**0.059**
M2	C1-M2-12	0.35	0.3	3	16	16.70	14.20	19.10	**0.056**

Fig. 6 shows the effect of different design variables on the maximum strain. Fig. 6a depicts the effect of L_1 and L_2 on the maximum strain. This figure shows the maximum strain to be almost insensitive to L_1. In this regard, results in Table S5.1 and Table S5.2 (in Supplementary Material-5) show that the strut thickness does not influence the maximum deformation in the stent during crimping. On the contrary, the graph shows that the larger the value of L_2 the lower the maximum strain, indicating that a lower number of cells helps in reducing the maximum strain during crimping. This is further demonstrated in Fig. 6b. The figure indicates that reducing the number of cells in the stent design from 5 to 3 reduces the maximum strain of about 30% for 16 pattern repetitions and 33% for 10 pattern repetitions. Fig. 6b also shows that for a given number of cells, the larger the number of pattern repetitions, the lower the maximum strain during crimping. Further, the influence of the number of pattern repetitions is more significant as the number of cells increases, with a 7% reduction for three cells and a 14% reduction in the case of five cells. However, the results indicate that, in general, the number of pattern repetitions has a lower impact on the maximum strain as compared to the number of cells. Fig. 6c shows the effect of the material. The figure shows that with material M1, the stent reaches larger strains during crimping than with material M2 (average value of 0.09 compared to 0.076, respectively).

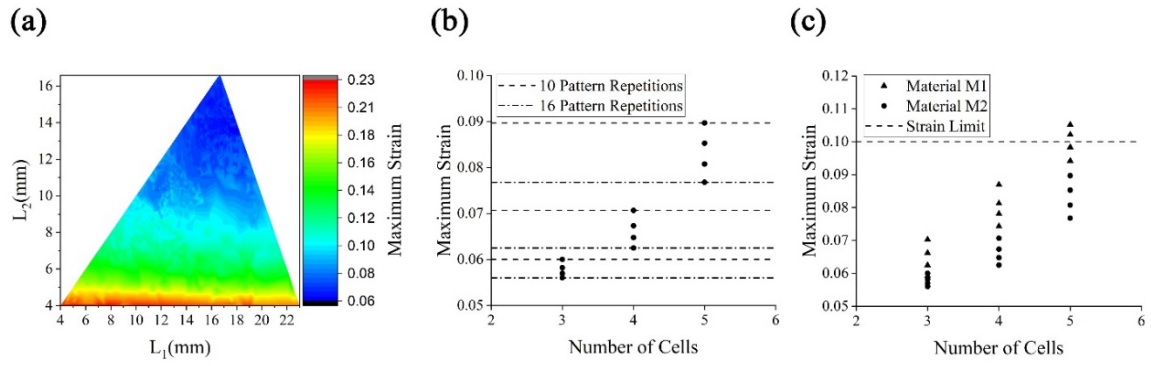

Fig. 6. Sensitivity of the maximum strain to different design variables, with width and thickness of 0.35 mm and 0.3 mm, respectively. a) The contour of the objective function as a function of cell dimension L_1 and L_2; b) Maximum strain as a function of the number of cells (dashed and dashed-dotted lines indicate the minimum and the maximum number of pattern repetitions considered); c) Maximum strain as a function of the number of cells for different materials

For all case scenarios, and independent of the material formulation, a linear relationship between the optimal L_1 (the length of the first cell) and stent height to the number of cells, $^{H}/_{n}$ was found, as shown in Fig. 7.

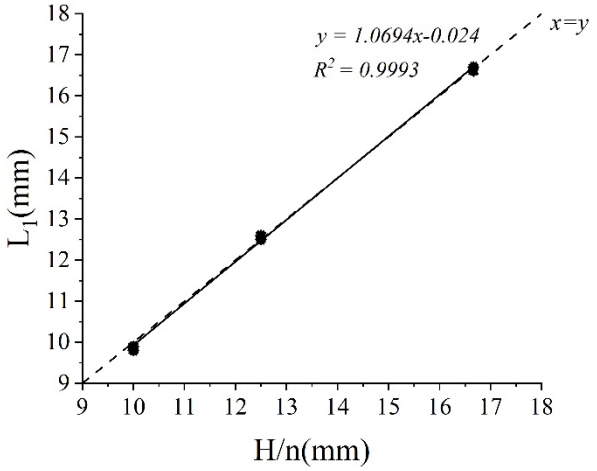

Fig. 7. For all cases, the design parameter L_1 is approximately equal to the height of the stent divided by the number of cells.

3.2 Evaluation of the optimization results using 3D simulation

To verify the ability of the simplified 1D string model to simulate the stent crimping, three different stent configurations with the same material model M2 and strut cross-section (0.35 mm × 0.3 mm)

were selected to compare the results in terms of the maximum strain with full 3D models of the stent. The three cases considered were: i) a model with 5 cells and 10 pattern repetitions (C1-M2-1) which showed the worst performance in terms of maximum strain (for the given strut cross-section); ii) a model with 4 cells and 12 pattern repetitions (C1-M2-6) corresponding to a design with a maximum strain in between the worst case and the optimum case; and iii) a model with 3 cells and 16 pattern repetitions (C1-M2-12), which corresponds to the optimal model (for the given strut cross-section). The 3D geometry of stents was created using the optimized values for L_1 and L_2 obtained with the optimization algorithm (see Table S5.2).

The comparison between the 1D and 3D simulations in terms of the maximum strain for the same stent models is depicted in Fig. 8. The maximum strain in the 3D model was obtained by calculating the average of maximum strain in all strings. Coinciding with the 1D simulations, the maximum strain in the 3D models occurred near the strut end. The difference between the average maximum strain in the 3D simulations and that in the simplified 1D string model of the stent was less than 5%. The simplified 1D string model, in general, underestimates the maximum strain value with respect to the 3D simulations.

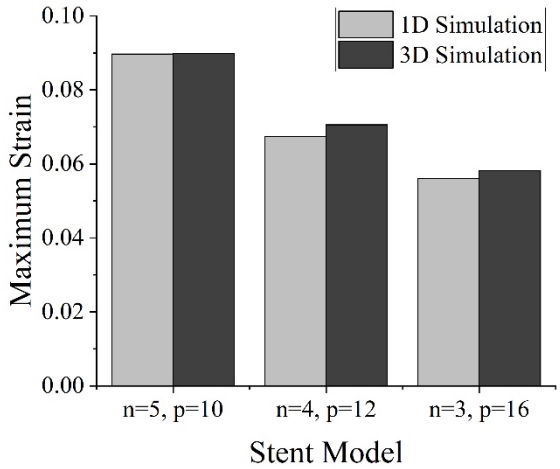

Fig. 8. The maximum strain in 3D simulation, dark columns, for the optimized stent configuration is consistent with the maximum strain calculated for the 1D string models, light grey column. The figure shows results for stent configurations with different number of cells (*n*) and different number of repeating patterns (*p*).

The 3D simulations have also allowed us to compare the total elongation of the stent during crimping. The 3D simulations gave 21.08%, 10.92%, and 4.72% elongations for models C1-M2-1, C1-M2-6, and C1-M2-12, respectively. These results compared favorably with 19.86%, 10.03%, and 3.31% obtained with the simplified 1D string model, which as in the case of the maximum strain, underestimates the total elongation of the stent. These results also indicate that the stent elongation during crimping increases with the number of cells.

To have a complete picture of the influence of the geometric parameters on the stent performance, departing from the optimal model for material M2, a sensitivity analysis of the radial force–diameter response, obtained as a by-product of the 3D simulations, to changes in the number of cells, pattern repetitions, and strut thickness and width was performed (a total of eight additional 3D simulations were performed). Fig. 9 shows the main results of the sensitivity analysis.

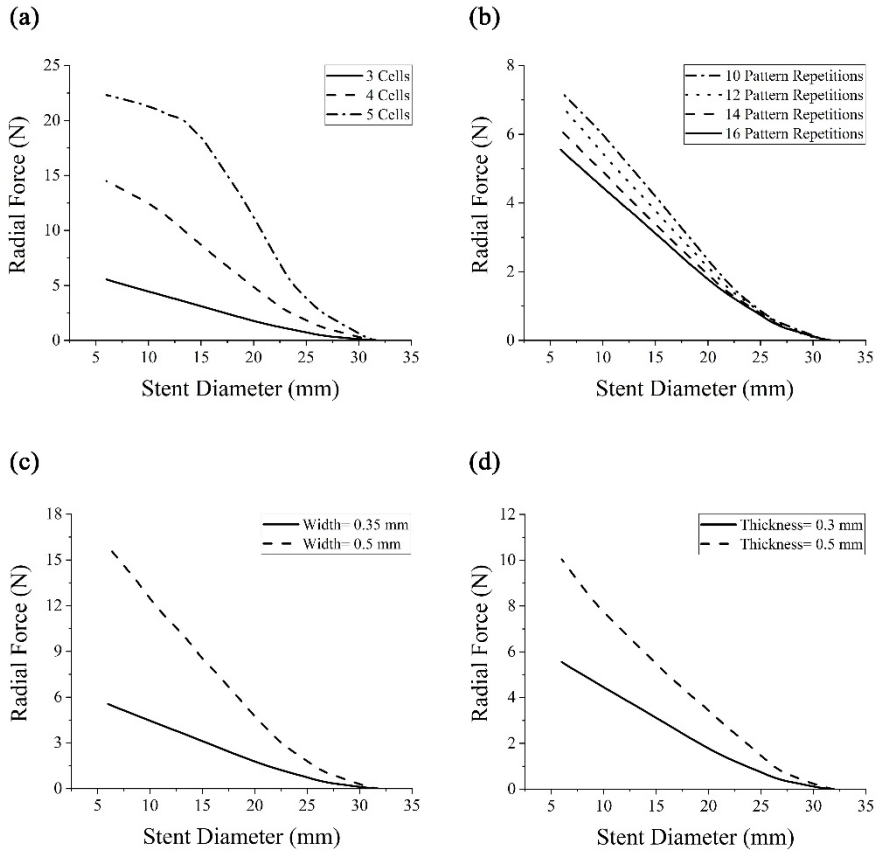

Fig. 9. Radial force–diameter curve as a function of different design variables. a) Models with the same number of pattern repetitions (p=16), strut width (w=0.35 mm), and strut thickness (t=0.3 mm), but a different number of cells. b) Models with w=0.35 mm, t=0.3 mm, n=3 and different number of pattern repetitions. c) Models with n=3, p=16, t=0.3 mm and different strut width. d) Models with n=3, p=16, w=0.35 mm, and different strut thickness.

In general, the results in Fig. 9 are consistent with the behavior of the radial force–diameter curves of Ni-Ti stents reported in the literature [18]. Regarding the sensitivity analysis, a 4-fold increment in the radial force is obtained when the number of cells increases from 3 to 5 (Fig. 9a). Besides, reducing the number of cells also modifies the shape of the radial force–diameter curve that changes from a sigmoidal to a linear response. On the contrary, reducing the number of pattern repetitions from 16 to 10 implies an increase in the maximum radial force of about 30% (Fig. 9b), indicating the significant effect of the number of cells in the overall stent stiffness. Regarding the

strut cross-section, Fig. 9c shows that increasing the strut width from 0.3 mm to 0.5 mm implies a 3-fold increment in the radial force, whereas a similar increment in the strut thickness only increases the maximum radial force by 80%.

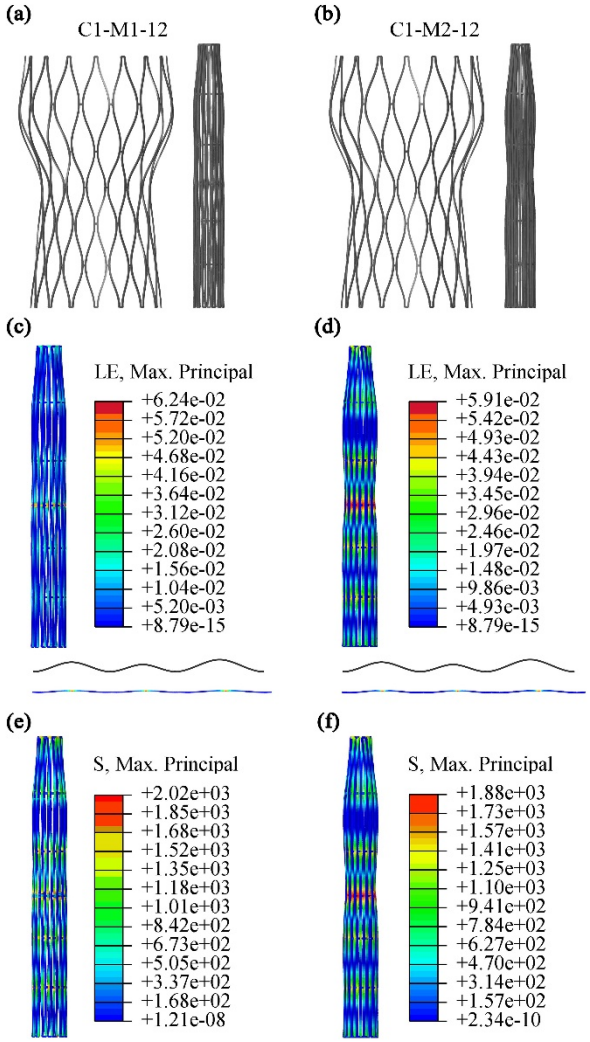

Fig. 10. The stress and strain distribution of the optimized models (w=0.35 mm, t=0.3 mm, n=3, p=16) for both M1 and M2 material properties after crimping to the diameter of 6 mm. a) Initial and crimped geometry of the optimized stent C1-M1-12; b) Initial and crimped states of the optimized stent model C1-M2-12; c)Strain contours of 3D and surrogate simulation of C1-M1-12; d) Strain contours of 3D and surrogate model of case C1M2-12; e) Stress distribution of C1-M1-12; f) Stress contour of model C1-M2-12

These additional simulations have allowed for further verification of the 1D string model with respect to the 3D model of the stent. In all cases, the difference in the average maximum strain between the two models was less than 5%, with comparable values of the maximum elongation as previously demonstrated (details given in Table S6.1 in the Supplementary Material-6). Fig. 10 demonstrates the strain and stress distribution in the optimized models of C1-M1-12 and C1-M2-12. The Maximum strain for both 1D and 3D models is observed in the same region (middle link of the second cell in this case) independent of the material properties. Besides, the strain in the regions close to the endpoints of the surrogate model is overestimated compared to the 3D model because of the different boundary conditions set for these models. In general, the material properties did not change the localization of the maximum strain as well as the optimal stent geometry, while the amount of maximum strain and stress in the model with M1 material properties is higher than the model with M2 material properties.

4 Discussion

In this study, a novel optimization approach for TAV stents based on the single repeating unit of the stent rather than on the full 3D representation of the stent has been proposed to reduce the maximum strain reached during the crimping procedure. To the best of our knowledge, this study is the first to present a framework for optimizing the TAV stent crimping process using a cost-effective, reliable approach considering six design variables. The optimization results demonstrated the variations of the maximum strain created in the stent as a significant factor in the crimping phase, with design parameters including width, thickness, number of cells and pattern repetitions, and the cell size. The proposed method provides a more simplistic, cost-effective, and accurate approach for evaluating the new TAV stent designs and helps to improve them to lower

the cost and risk of the clinical evaluations. Stent design requirements are usually antagonists. It is demonstrated in our study and literature that changing one parameter in favor of improving one functional aspect usually leads to compromise the structural performance [25,50].

The simplified stent model. One of the novelties of this work is using a simplified representation of the stent (a surrogate) to drive the optimization process. This strategy has been demonstrated to be computationally efficient by reducing the computational time in more than three orders of magnitude with respect to the 3D simulations. However, a detailed comparison of the maximum strain and stent elongation during crimping shows that the surrogate model underestimates these values. Hence, performing an optimization based on the maximum strain and possibly the maximum stent elongation may require imposing stringent limits for these values when using the 1D string model to guarantee that they are respected in the full 3D model. Our results demonstrate that a 10% reduction in the allowable values is sufficient when using the surrogate model.

Effect of the cell size. In all stent models provided in this study, the length of each cell of the stent was optimized to find the design with the least maximum strain. The cell size, especially the size of the intermediate cells, characterized by the parameter L_2, has a remarkable effect on the maximum strain in the stent during crimping, Fig. 6a. On the contrary, the optimal length of the first cell (L_1) was found to correlate linearly with the stent height to the number of cells ratio (Fig. 7). This result permits a quick estimation of these geometric parameters, allowing a further reduction in the optimization cost and speeding up the whole design process. In addition, the size of the first cell has been reported to have an important role in the hemodynamics and fatigue behavior of the stent [40].

Effect of the number of cells and pattern repetitions. The number of cells has a pivotal role in minimizing the maximum strain during crimping and the maximal radial force exerted by the stent.

In fact, for a fixed number of pattern repetitions, changing the number of cells from 5 to 3 may reduce the maximum strain up to 33%. The reason for this behavior is that, as the number of cells increases, the stretch of the stent increases during crimping, implying a larger deformation of the struts. However, the most remarkable effect of the number of cells is found on the maximum radial force of the stent. Reducing the number of cells from 5 to 3, the maximal radial force reduces 4-fold, consistent with what was reported in [12].

Concerning the number of pattern repetitions, the effect is the opposite. Increasing the number of pattern repetitions from 10 to 16 reduces the maximum strain up to 14% and the radial force by 25%. This behavior is associated with the shape of the cell and the overall stiffness of the stent. For a fixed number of pattern repetitions, as the number of cells increases, the in-plane (longitudinal) bending stiffness of the cell strut increases as it becomes shorter, leading to larger radial forces, as observed in Fig. 9a. On the contrary, for a fixed number of cells, as the number of pattern repetitions decreases, the maximum curvature on each single cell increases leading to a larger bending stiffness and, therefore, larger radial forces (see Fig. 9b).

The results state that a smaller number of cells and a larger number of patterns contribute to reducing the maximum strain during crimping. This result is in agreement with the work in [53], which reports that an increment in the number of patterns improves the safety factor against the yielding of the stent. Thus, a higher number of pattern repetitions is in favor of strain levels and plasticization safety, implying better performance against fatigue. In addition, the larger the number of pattern repetitions, the lower the maximum radial force delivered by the stent.

Effect of the strut width and thickness. The change in strut width had a significant impact on the maximum strain achieved during crimping. However, changes in strut thickness were found not to affect the strain level. In fact, changing the strut width from 0.35 mm to 0.5 mm in the

optimal stent configuration resulted in a 33% increase in the maximum strain, whereas increasing the strut thickness from 0.35 mm to 0.5 mm changed the maximum strain by less than 0.5%. This behavior demonstrates that during crimping, most of the mechanical work is associated with in-plane bending of the struts that align the struts with the longitudinal direction of the stent. Therefore, increasing the width of the strut increases the in-plane bending stiffness leading to larger radial forces. In this study, we have assumed the thickness and width as constant. In commercial stents, the local thickness and width may vary along the stent as a consequence of the fabrication process. However, the variations are expected to be small with respect to the nominal value. In addition, an accurate estimation of this local variation will require simulating the entire fabrication process of the stent, which is out of the scope of this work.

Effect of the material properties. The two material properties used for the simulations considerably impacted the maximum strain during crimping and the delivered radial force, even though they render almost identical optimized shapes for the stent, Table 3 and Fig. 10. The differences in the maximum strain were associated with the symmetric behavior in traction and compression of both materials. For material M1, which considers an asymmetry in traction and compression, in the cases with a large number of cells (n=5), the optimization of the cell geometry could not guarantee a maximum strain below the yielding limit. These results point to the importance of the design of the mechanical properties of the Ni-Ti alloys. An incorrect selection of the mechanical properties could render a stent design inappropriate in terms of the yielding limit or the delivered radial force [12,54]. However, the geometry of the optimized stent for both materials was identical, indicating that the mechanical characteristics of the Ni-Ti alloy do not influence the optimal geometric features of the stent.

The results of this study show that, in general, minimizing the maximum strain to prevent yielding during the crimping phase may reduce the stent's maximum radial force, which may limit its ability to open highly calcified valves during the deployment phase. On the contrary, lower radial forces will cause lower contact forces against the septum and the aorta, reducing the probability of inducing conduction abnormalities after valve implantation, i.e., a left bundle branch block and tissue damage in the artery [51,52]. In the cases with material M2, considering best and worst-case scenarios regarding the maximum strain (C1-M2-12 and C4-M2-37), a 52% reduction in the maximum strain and a 17 fold reduction of the maximum radial force exist between these models. The case C4-M2-37 has a maximum crimping strain of 0.117 which exceeds the material yielding limit (0.1 in our study) by 17%. Therefore, designing the self-expandable stents requires a compromise between minimizing the maximum strain in the stent while keeping the maximum radial force delivered by the device during deployment as high as possible. Hence, when choosing the design parameters, it is necessary to consider the need to crimp the stent to fit in an 18Fr catheter without causing yielding in the stent while providing a minimal radial force that guarantees the success of the intervention while preventing excessive tissue damage.

This study is not exempt from limitations. The optimization in this study concentrated only on crimping strain minimization to prevent yielding. This criterion guarantees that the valve is not being permanently distorted during crimping and contributes to increasing the fatigue life of the device. However, other aspects regarding the performance of the valve are important in the valve design, i.e., hemodynamics behavior or the radial force–diameter response. In this regard, the presented framework can be easily adapted to incorporate additional elements in the objective function, i.e., minimizing the maximum strain while maximizing the maximum radial force of the stent or as constraints to further limit the design space. Further investigations are needed in

multidisciplinary approaches to include other stent design parameters, implantation steps, and functional factors, such as post-implantation anchorage, leakage and radial strength in the aortic root, fatigue resistance to achieve a more accurate and reliable design with improved overall performance.

5 Conclusion

This study presents the results of a novel optimization framework for minimizing the strain in TAV stents during the crimping procedure. It is one of the few studies investigating the design optimization of these stents, starting from evaluating a 1D representative string. The results have been then verified through 3D simulations. The results show that our proposed optimization method provides a cost-effective tool to evaluate the stent during crimping, compared to complex 3D simulations that are commonly used. Adding other design parameters, considering further steps of implanting the stent and other functional factors would lead to a more accurate and reliable design.

Acknowledgments The authors would like to thank Dr. Adelaide Nespoli and Dr. Elena Villa from CNR-ICMATE (Lecco), who performed the thermomechanical treatments and surface finishing on the raw material. The authors would like to thank also Dr. Ali Gokhan Demir from the Department of Mechanical Engineering of Politecnico di Milano for performing the laser cutting to obtain the specimens used in this work.

Declaration of competing interest None Declared.

Funding This research did not receive any specific grant from funding agencies in the public, commercial, or not-for-profit sectors.

References

[1] A. Cribier, H. Eltchaninoff, A. Bash, N. Borenstein, C. Tron, F. Bauer, G. Derumeaux, F. Anselme, F. Laborde, M.B. Leon, Percutaneous transcatheter implantation of an aortic valve prosthesis for calcific aortic stenosis: First human case description, Circulation. 106 (2002) 3006–3008. https://doi.org/10.1161/01.CIR.0000047200.36165.B8.

[2] M.J. Mack, M.B. Leon, C.R. Smith, D.C. Miller, J.W. Moses, E.M. Tuzcu, J.G. Webb, P.S. Douglas, W.N. Anderson, E.H. Blackstone, S.K. Kodali, R.R. Makkar, G.P. Fontana, S. Kapadia, J. Bavaria, R.T. Hahn, V.H. Thourani, V. Babaliaros, A. Pichard, H.C. Herrmann, D.L. Brown, M. Williams, M.J. Davidson, L.G. Svensson, J. Akin, 5-year outcomes of transcatheter aortic valve replacement or surgical aortic valve replacement for high surgical risk patients with aortic stenosis (PARTNER 1): A randomised controlled trial, Lancet. 385 (2015) 2477–2484. https://doi.org/10.1016/S0140-6736(15)60308-7.

[3] D.H. Adams, J.J. Popma, M.J. Reardon, S.J. Yakubov, J.S. Coselli, G.M. Deeb, T.G. Gleason, M. Buchbinder, J. Hermiller, N.S. Kleiman, S. Chetcuti, J. Heiser, W. Merhi, G. Zorn, P. Tadros, N. Robinson, G. Petrossian, G.C. Hughes, J.K. Harrison, J. Conte, B. Maini, M. Mumtaz, S. Chenoweth, J.K. Oh, Transcatheter Aortic-Valve Replacement with a Self-Expanding Prosthesis, N. Engl. J. Med. 370 (2014). https://doi.org/10.1056/NEJMoa1400590.

[4] J.P. Fanning, D.G. Platts, D.L. Walters, J.F. Fraser, Transcatheter aortic valve implantation (TAVI): valve design and evolution., Int. J. Cardiol. 168 (2013) 1822–31. https://doi.org/10.1016/j.ijcard.2013.07.117.

[5] S.C. Malaisrie, A. Iddriss, J.D. Flaherty, A. Churyla, Transcatheter Aortic Valve Implantation, Curr. Atheroscler. Rep. 18 (2016) 27. https://doi.org/10.1007/s11883-016-0577-2.

[6] D. Todaro, A. Picci, M. Barbanti, Technical characteristics and evidence to date for FDA- and CE Mark-approved valves, Interv. Today. 11 (2017) 53–58. https://citoday.com/pdfs/cit0317_F5_Barbanti.pdf.

[7] J. Rodés-Cabau, Transcatheter aortic valve implantation: current and future approaches, Nat. Rev. Cardiol. 9 (2011) 15–29. https://doi.org/10.1038/nrcardio.2011.164.

[8] G.A. Fishbein, F.J. Schoen, M.C. Fishbein, Transcatheter aortic valve implantation: Status and challenges, Cardiovasc. Pathol. 23 (2014) 65–70. https://doi.org/10.1016/j.carpath.2013.10.001.

[9] R.A. Siemieniuk, T. Agoritsas, V. Manja, T. Devji, Y. Chang, M.M. Bala, L. Thabane, G.H. Guyatt, Transcatheter versus surgical aortic valve replacement in patients with severe aortic stenosis at low and intermediate risk: Systematic review and meta-analysis, BMJ. 354 (2016). https://doi.org/10.1136/bmj.i5130.

[10] T.K. Rosengart, T. Feldman, M.A. Borger, T.A. Vassiliades, A.M. Gillinov, K.J. Hoercher, A. Vahanian, R.O. Bonow, W. O'Neill, Percutaneous and minimally invasive valve procedures: A scientific statement from the American Heart Association Council on Cardiovascular Surgery and Anesthesia, Council on Clinical Cardiology, Functional

Genomics and Translational Biology Interdisciplin, Circulation. 117 (2008) 1750–1767. https://doi.org/10.1161/CIRCULATIONAHA.107.188525.

[11] N. Perrin, A. Frei, S. Noble, Transcatheter aortic valve implantation: Update in 2018, Eur. J. Intern. Med. 55 (2018) 12–19. https://doi.org/10.1016/j.ejim.2018.07.002.

[12] M.S. Cabrera, C.W.J. Oomens, F.P.T. Baaijens, Understanding the requirements of self-expandable stents for heart valve replacement: Radial force, hoop force and equilibrium, J. Mech. Behav. Biomed. Mater. 68 (2017) 252–264. https://doi.org/10.1016/j.jmbbm.2017.02.006.

[13] T.W. Duerig, D.E. Tolomeo, M. Wholey, An overview of superelastic stent design, Minim. Invasive Ther. Allied Technol. 9 (2000) 235–246. https://doi.org/10.4028/www.scientific.net/MSF.394-395.1.

[14] Y. Xuan, D. Dvir, Z. Wang, T. Mizoguchi, J. Ye, J.M. Guccione, L. Ge, E.E. Tseng, Stent and leaflet stresses in 26-mm, third-generation, balloon-expandable transcatheter aortic valve, J. Thorac. Cardiovasc. Surg. 157 (2019) 528–536. https://doi.org/10.1016/j.jtcvs.2018.04.115.

[15] G. Rocatello, N. El Faquir, G. De Santis, F. Iannaccone, J. Bosmans, O. De Backer, L. Sondergaard, P. Segers, M. De Beule, P. De Jaegere, P. Mortier, Patient-Specific Computer Simulation to Elucidate the Role of Contact Pressure in the Development of New Conduction Abnormalities after Catheter-Based Implantation of a Self-Expanding Aortic Valve, Circ. Cardiovasc. Interv. 11 (2018) e005344. https://doi.org/10.1161/CIRCINTERVENTIONS.117.005344.

[16] F. Migliavacca, L. Petrini, V. Montanari, I. Quagliana, F. Auricchio, G. Dubini, A predictive study of the mechanical behaviour of coronary stents by computer modelling, Med. Eng. Phys. 27 (2005) 13–18. https://doi.org/10.1016/j.medengphy.2004.08.012.

[17] A.R. Pelton, V. Schroeder, M.R. Mitchell, X.Y. Gong, M. Barney, S.W. Robertson, Fatigue and durability of Nitinol stents, J. Mech. Behav. Biomed. Mater. 1 (2008) 153–164. https://doi.org/10.1016/j.jmbbm.2007.08.001.

[18] C. Kleinstreuer, Z. Li, C.A. Basciano, S. Seelecke, M.A. Farber, Computational mechanics of Nitinol stent grafts, J. Biomech. 41 (2008) 2370–2378. https://doi.org/10.1016/j.jbiomech.2008.05.032.

[19] H. Zahedmanesh, D. John Kelly, C. Lally, Simulation of a balloon expandable stent in a realistic coronary artery-Determination of the optimum modelling strategy, J. Biomech. 43 (2010) 2126–2132. https://doi.org/10.1016/j.jbiomech.2010.03.050.

[20] L. Lei, X. Qi, S. Li, Y. Yang, Y. Hu, B. Li, S. Zhao, Y. Zhang, Finite element analysis for fatigue behaviour of a self-expanding Nitinol peripheral stent under physiological biomechanical conditions, Comput. Biol. Med. 104 (2019) 205–214. https://doi.org/10.1016/j.compbiomed.2018.11.019.

[21] G. Alaimo, F. Auricchio, M. Conti, M. Zingales, Multi-objective optimization of nitinol stent design, Med. Eng. Phys. 47 (2017) 13–24. https://doi.org/10.1016/j.medengphy.2017.06.026.

[22] S. Tammareddi, G. Sun, Q. Li, Multiobjective robust optimization of coronary stents, Mater. Des. 90 (2016) 682–692. https://doi.org/10.1016/j.matdes.2015.10.153.

[23] A. Amirjani, M. Yousefi, M. Cheshmaroo, Parametrical optimization of stent design; A numerical-based approach, Comput. Mater. Sci. 90 (2014) 210–220. https://doi.org/10.1016/j.commatsci.2014.04.002.

[24] M. Azaouzi, N. Lebaal, A. Makradi, S. Belouettar, Optimization based simulation of self-expanding nitinol stent, Lect. Notes Mech. Eng. 1 (2013) 423–450. https://doi.org/10.1007/978-3-642-37143-1_50.

[25] S. Pant, G. Limbert, N.P. Curzen, N.W. Bressloff, Multiobjective design optimisation of coronary stents, Biomaterials. 32 (2011) 7755–7773. https://doi.org/10.1016/j.biomaterials.2011.07.059.

[26] N.K. Putra, P.S. Palar, H. Anzai, K. Shimoyama, M. Ohta, Multiobjective design optimization of stent geometry with wall deformation for triangular and rectangular struts, Med. Biol. Eng. Comput. 57 (2019) 15–26. https://doi.org/10.1007/s11517-018-1864-6.

[27] N.S. Ribeiro, J. Folgado, H.C. Rodrigues, Surrogate-based visualization and sensitivity analysis of coronary stent performance: A study on the influence of geometric design, Int. j. Numer. Method. Biomed. Eng. 34 (2018) e3125. https://doi.org/10.1002/cnm.3125.

[28] J.K. Forrest, A.A. Mangi, J.J. Popma, K. Khabbaz, M.J. Reardon, N.S. Kleiman, S.J. Yakubov, D. Watson, S. Kodali, I. George, P. Tadros, G.L. Zorn, J. Brown, R. Kipperman, S. Saul, H. Qiao, J.K. Oh, M.R. Williams, Early Outcomes With the Evolut PRO Repositionable Self-Expanding Transcatheter Aortic Valve With Pericardial Wrap, JACC Cardiovasc. Interv. 11 (2018) 160–168. https://doi.org/10.1016/j.jcin.2017.10.014.

[29] T.E. Feldman, M.J. Reardon, V. Rajagopal, R.R. Makkar, T.K. Bajwa, N.S. Kleiman, A. Linke, D.J. Kereiakes, R. Waksman, V.H. Thourani, R.C. Stoler, G.J. Mishkel, D.G. Rizik, V.S. Iyer, T.G. Gleason, D. Tchétché, J.D. Rovin, M. Buchbinder, I.T. Meredith, M. Götberg, H. Bjursten, C. Meduri, M.H. Salinger, D.J. Allocco, K.D. Dawkins, Effect of mechanically expanded vs self-expanding transcatheter aortic valve replacement on mortality and major adverse clinical events in high-risk patients with aortic stenosis the REPRISE III randomized clinical trial, JAMA - J. Am. Med. Assoc. 319 (2018) 27–37. https://doi.org/10.1001/jama.2017.19132.

[30] M.J. Mack, M.B. Leon, V.H. Thourani, R. Makkar, S.K. Kodali, M. Russo, S.R. Kapadia, S. Chris Malaisrie, D.J. Cohen, P. Pibarot, J. Leipsic, R.T. Hahn, P. Blanke, M.R. Williams, J.M. McCabe, D.L. Brown, V. Babaliaros, S. Goldman, W.Y. Szeto, P. Genereux, A. Pershad, S.J. Pocock, M.C. Alu, J.G. Webb, C.R. Smith, Transcatheter aortic-valve replacement with a balloon-expandable valve in low-risk patients, N. Engl. J. Med. 380 (2019) 1695–1705. https://doi.org/10.1056/NEJMoa1814052.

[31] J.J. Popma, G. Michael Deeb, S.J. Yakubov, M. Mumtaz, H. Gada, D. O'Hair, T. Bajwa, J.C. Heiser, W. Merhi, N.S. Kleiman, J. Askew, P. Sorajja, J. Rovin, S.J. Chetcuti, D.H. Adams, P.S. Teirstein, G.L. Zorn, J.K. Forrest, D. Tchétché, J. Resar, A. Walton, N. Piazza, B. Ramlawi, N. Robinson, G. Petrossian, T.G. Gleason, J.K. Oh, M.J. Boulware, H. Qiao, A.S. Mugglin, M.J. Reardon, Transcatheter aortic-valve replacement with a self-expanding

valve in low-risk patients, N. Engl. J. Med. 380 (2019) 1706–1715. https://doi.org/10.1056/NEJMoa1816885.

[32] M.J. Reardon, T.E. Feldman, C.U. Meduri, R.R. Makkar, D. O'Hair, A. Linke, D.J. Kereiakes, R. Waksman, V. Babliaros, R.C. Stoler, G.J. Mishkel, D.G. Rizik, V.S. Iyer, T.G. Gleason, D. Tchétché, J.D. Rovin, T. Lhermusier, D. Carrié, R.W. Hodson, D.J. Allocco, I.T. Meredith, Two-Year Outcomes after Transcatheter Aortic Valve Replacement with Mechanical vs Self-expanding Valves: The REPRISE III Randomized Clinical Trial, JAMA Cardiol. 4 (2019) 223–229. https://doi.org/10.1001/jamacardio.2019.0091.

[33] P. Blanke, J.A. Leipsic, J.J. Popma, S.J. Yakubov, G.M. Deeb, H. Gada, M. Mumtaz, B. Ramlawi, N.S. Kleiman, P. Sorajja, J. Askew, C.U. Meduri, J. Kauten, S. Melnitchouk, I. Inglessis, J. Huang, M. Boulware, M.J. Reardon, Bioprosthetic Aortic Valve Leaflet Thickening in the Evolut Low Risk Sub-Study, J. Am. Coll. Cardiol. 75 (2020) 2430–2442. https://doi.org/10.1016/j.jacc.2020.03.022.

[34] E.A. Ovcharenko, K.U. Klyshnikov, A.E. Yuzhalin, G. V Savrasov, A.N. Kokov, A. V. Batranin, V.I. Ganyukov, Y.A. Kudryavtseva, Modeling of transcatheter aortic valve replacement: Patient specific vs general approaches based on finite element analysis, Comput. Biol. Med. 69 (2016) 29–36. https://doi.org/10.1016/j.compbiomed.2015.12.001.

[35] W. Mao, K. Li, W. Sun, Fluid–Structure Interaction Study of Transcatheter Aortic Valve Dynamics Using Smoothed Particle Hydrodynamics, Cardiovasc. Eng. Technol. 7 (2016) 374–388. https://doi.org/10.1007/s13239-016-0285-7.

[36] S. Tzamtzis, J. Viquerat, J. Yap, M.J. Mullen, G. Burriesci, Medical Engineering & Physics Numerical analysis of the radial force produced by the Medtronic-CoreValve and Edwards-SAPIEN after transcatheter aortic valve implantation (TAVI), Med. Eng. Phys. 35 (2013) 125–130. https://doi.org/10.1016/j.medengphy.2012.04.009.

[37] R.P. Ghosh, G. Marom, M. Bianchi, K. D'souza, W. Zietak, D. Bluestein, Numerical evaluation of transcatheter aortic valve performance during heart beating and its post-deployment fluid–structure interaction analysis, Biomech. Model. Mechanobiol. 19 (2020) 1725–1740. https://doi.org/10.1007/s10237-020-01304-9.

[38] S. Pasta, S. Cannata, G. Gentile, M. Di Giuseppe, F. Cosentino, F. Pasta, V. Agnese, D. Bellavia, G.M. Raffa, M. Pilato, C. Gandolfo, Simulation study of transcatheter heart valve implantation in patients with stenotic bicuspid aortic valve, Med. Biol. Eng. Comput. 58 (2020) 815–829. https://doi.org/10.1007/s11517-020-02138-4.

[39] G. Luraghi, F. Migliavacca, A. García-González, C. Chiastra, A. Rossi, D. Cao, G. Stefanini, J.F. Rodriguez Matas, On the Modeling of Patient-Specific Transcatheter Aortic Valve Replacement: A Fluid–Structure Interaction Approach, Cardiovasc. Eng. Technol. 10 (2019) 437–455. https://doi.org/10.1007/s13239-019-00427-0.

[40] G. Rocatello, G. De Santis, S. De Bock, M. De Beule, P. Segers, P. Mortier, Optimization of a Transcatheter Heart Valve Frame Using Patient-Specific Computer Simulation, Cardiovasc. Eng. Technol. 10 (2019) 456–468. https://doi.org/10.1007/s13239-019-00420-7.

[41] G.M. Bosi, C. Capelli, M.H. Cheang, N. Delahunty, M. Mullen, A.M. Taylor, S. Schievano,

Population-specific material properties of the implantation site for transcatheter aortic valve replacement finite element simulations, J. Biomech. 71 (2018) 236–244. https://doi.org/10.1016/j.jbiomech.2018.02.017.

[42] D. Carbonaro, D. Gallo, U. Morbiducci, A. Audenino, C. Chiastra, In silico biomechanical design of the metal frame of transcatheter aortic valves: multi-objective shape and cross-sectional size optimization, Struct. Multidiscip. Optim. (2021). https://doi.org/10.1007/s00158-021-02944-w.

[43] F. Auricchio, R.L. Taylor, J. Lubliner, Shape-memory alloys: Macromodelling and numerical simulations of the superelastic behavior, Comput. Methods Appl. Mech. Eng. 146 (1997) 281–312. https://doi.org/10.1016/S0045-7825(96)01232-7.

[44] E. Dordoni, L. Petrini, W. Wu, F. Migliavacca, G. Dubini, G. Pennati, Computational Modeling to Predict Fatigue Behavior of NiTi Stents: What Do We Need?, J. Funct. Biomater. 6 (2015) 299–317. https://doi.org/10.3390/jfb6020299.

[45] E. Dordoni, Fatigue analysis of Nitinol cardiovascular devices. PhD Thesis, Politecnico di Milano, 2014.

[46] L. Petrini, W. Wu, E. Dordoni, A. Meoli, F. Migliavacca, G. Pennati, Fatigue behavior characterization of nitinol for peripheral stents, Funct. Mater. Lett. 5 (2012). https://doi.org/10.1142/S1793604712500129.

[47] S.W. Robertson, A.R. Pelton, R.O. Ritchie, Mechanical fatigue and fracture of Nitinol, Http://Dx.Doi.Org/10.1179/1743280411Y.0000000009. 57 (2013) 1–36. https://doi.org/10.1179/1743280411Y.0000000009.

[48] L. Petrini, A. Bertini, F. Berti, G. Pennati, F. Migliavacca, The role of inelastic deformations in the mechanical response of endovascular shape memory alloy devices, Proc. Inst. Mech. Eng. Part H J. Eng. Med. 231 (2017) 391–404. https://doi.org/10.1177/0954411917696336.

[49] S. Shan, G.G. Wang, Survey of modeling and optimization strategies to solve high-dimensional design problems with computationally-expensive black-box functions, Struct. Multidiscip. Optim. 41 (2010) 219–241. https://doi.org/10.1007/s00158-009-0420-2.

[50] H. Li, J. Gu, M. Wang, D. Zhao, Z. Li, A. Qiao, B. Zhu, Multi-objective optimization of coronary stent using Kriging surrogate model, Biomed. Eng. Online. 15 (2016) 275–291. https://doi.org/10.1186/s12938-016-0268-9.

[51] G. Rocatello, N. El Faquir, G. De Santis, F. Iannaccone, J. Bosmans, O. De Backer, L. Sondergaard, P. Segers, M. De Beule, P. De Jaegere, P. Mortier, Patient-Specific Computer Simulation to Elucidate the Role of Contact Pressure in the Development of New Conduction Abnormalities after Catheter-Based Implantation of a Self-Expanding Aortic Valve, Circ. Cardiovasc. Interv. 11 (2018) 1–9. https://doi.org/10.1161/CIRCINTERVENTIONS.117.005344.

[52] A. Finotello, R.M. Romarowski, R. Gorla, G. Bianchi, F. Bedogni, F. Auricchio, S. Morganti, Performance of high conformability vs. high radial force devices in the virtual treatment of TAVI patients with bicuspid aortic valve, Med. Eng. Phys. 89 (2021) 42–50. https://doi.org/10.1016/j.medengphy.2021.02.004.

[53] E. Masoumi Khalil Abad, D. Pasini, R. Cecere, Shape optimization of stress concentration-free lattice for self-expandable Nitinol stent-grafts, J. Biomech. 45 (2012) 1028–1035. https://doi.org/10.1016/j.jbiomech.2012.01.002.

[54] A. Finotello, R. Gorla, N. Brambilla, F. Bedogni, F. Auricchio, S. Morganti, Finite element analysis of transcatheter aortic valve implantation: Insights on the modelling of self-expandable devices, J. Mech. Behav. Biomed. Mater. 123 (2021) 104772. https://doi.org/10.1016/j.jmbbm.2021.104772.